Entropy-Driven Design of Highly Impact-Stiffening Supramolecular Polymer Networks with Salt-Bridge Hydrogen Bonds

Haiyan Qiao, Baohu Wu, Shengtong Sun,* and Peiyi Wu*

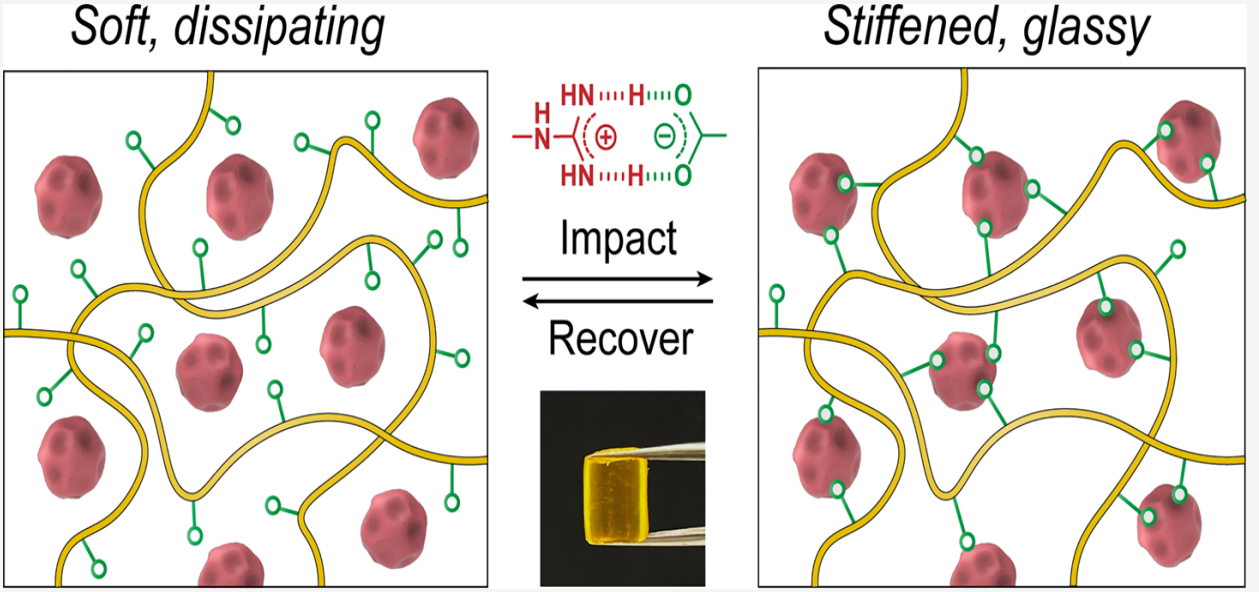

ABSTRACT: Impact-stiffening materials that undergo a strain rate-induced soft-to-rigid transition hold great promise as soft armors in the protection of the human body and equipment. However, current impact-stiffening materials, such as polyborosiloxanes and shear-thickening fluids, often exhibit a limited impact-stiffening response. Herein, we propose a design strategy for fabricating highly impact-stiffening supramolecular polymer networks by leveraging high-entropy-penalty physical interactions. We synthesized a fully biobased supramolecular polymer comprising poly(α-thioctic acid) and arginine clusters, whose chain dynamics are governed by highly specific guanidinium-carboxylate salt-bridge hydrogen bonds. The resulting material exhibits an exceptional impact-stiffening response of ~2100 times, transitioning from a soft dissipating state (21 kPa, 0.1 Hz) to a highly stiffened glassy state (45.3 MPa, 100 Hz) with increasing strain rates. Moreover, the material's high energy-dissipating and hot-melting properties bring excellent damping performance and easy hybridization with other scaffolds. This entropy-driven approach paves the way for the development of next-generation soft, sustainable, and impact-resistant materials.

INTRODUCTION

Impact-resistant materials play a vital role in the protection of the human body, apparatus, robotics, and aerospace structures.[1] To survive the impact, a material must exhibit high strength and toughness at high strain rates to effectively dissipate the kinetic impact energy. A prevalent approach involves designing high-energy-dissipating materials via various toughening mechanisms, such as bioinspired multilayer or bouligand assemblies,[2−6] fiber reinforcement,[7−9] phase separation,[10,11] and molecular clogging.[12] However, the intrinsic rigidity of these materials greatly restricts their applicability in modern wearable and buffering scenarios, which demand adaptability and compliance with the moving human body or underlying objects. To address this challenge, impact-stiffening materials have been developed as smart soft armors, retaining softness under quasi-static conditions while undergoing dramatic stiffening upon impact at high strain rates.[13] Two notable examples include polyborosiloxanes (PBSs) or Silly Putty, which rely on rate-dependent B−O dative bonds,[14] and shear-thickening fluids (e.g., cornstarch and silica suspensions), which operate based on a reentrant jamming transition.[15,16] To enhance their functionality, numerous efforts have focused on modifying their composition or hybridizing them with fillers/scaffolds.[17−22] Nevertheless, constrained by material type and rate-responsive mechanisms, the stiffening response of current impact-stiffening materials remains relatively low, with the storage modulus (G') increase generally less than 1000 times within the typical shear frequency range of 0.1−100 Hz.

Supramolecular polymer networks (SPNs), characterized by their highly dynamic cross-links, have emerged as a promising candidate for designing impact-stiffening materials.[23−27] Importantly, the kinetics of the transient physical interactions among supramolecular polymer chains are highly sensitive to strain rate, enabling the rapid soft-to-rigid transformation upon

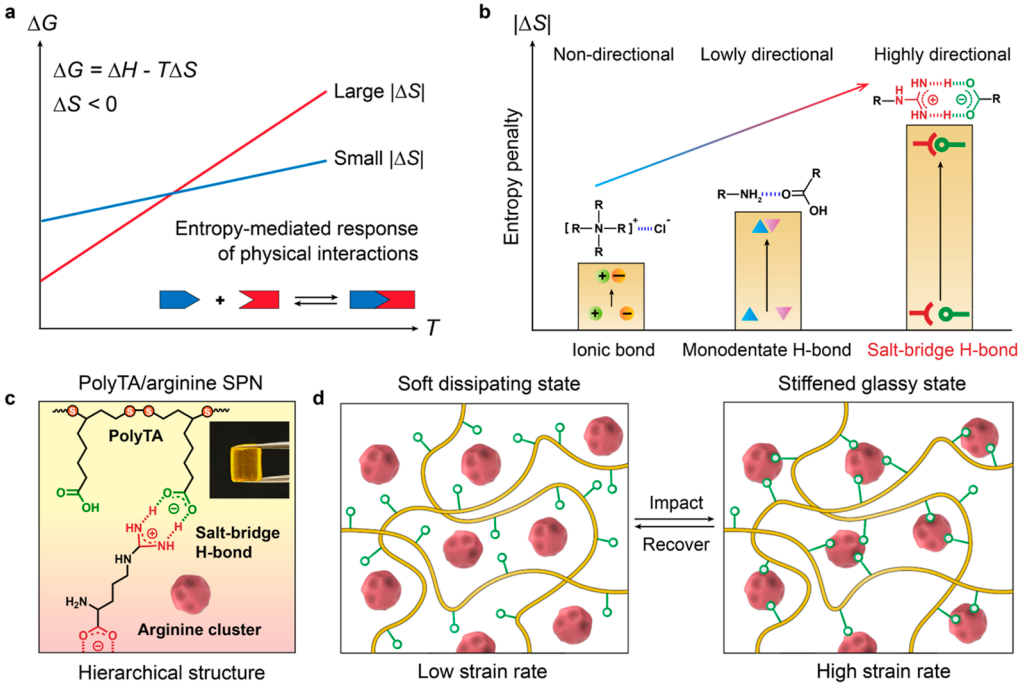

Figure 1. Working mechanism of the impact-stiffening SPN. (a) Thermodynamic interpretation for the stiffening response of the SPN as a function of temperature (or strain rate, according to the principle of time−temperature equivalency). The kinetics of transient physical interactions (depicted by Gibb's free energy, ΔG) are mediated by the entropy penalty ($|\Delta S|$), which is the slope of the $\Delta G-T$ curve. (b) Rough comparison of entropy penalties ($|\Delta S|$) among three typical interactions, involving an ionic bond (nondirectional), a monodentate H-bond (lowly directional), and a salt-bridge H-bond (highly directional). (c) Hierarchical structure of the polyTA/arginine SPN comprising arginine clusters and a polyTA matrix. The inset is a photograph of a cylinder SPN sample. (d) Schematic mechanism of the impact-stiffening polyTA/arginine SPN enabled by interfacial salt-bridge H-bonds. Upon impact, the material transitions rapidly from a soft dissipating state (cross-linked by weak interfacial H-bonds) to a highly stiffened glassy state (cross-linked by strong interfacial H-bonds). This process is fully reversible.

impact.[28,29] This strain rate dependence can be understood within a classical thermodynamic framework. As depicted in Figure 1a, the formation of typical physical interactions is often accompanied by an entropy penalty (loss of conformational entropy, $\Delta S < 0$).[30−32] Based on the principle of time−temperature equivalency, the strain rate dependence of transient cross-links in SPNs can be effectively regulated by manipulating the entropy penalty ($|\Delta S|$), which is the slope of the Gibbs free energy (ΔG)−temperature curve. Therefore, high-entropy-penalty physical interactions often lead to a high strain rate dependence of network dynamics and, thus, a more remarkable stiffening response. Such a framework may also explain the observed impact-stiffening effect of PBSs, which utilize directional B−O dative bonds with a high entropy penalty as the dominant cross-linkers.[33] Unfortunately, despite the abundance of physical interactions that can be exploited for molecular design, the potential of SPNs as impact-stiffening materials remains largely untapped.

In this work, we demonstrate the fabrication of highly impact-stiffening SPNs by harnessing the high-entropy-penalty salt-bridge hydrogen bond (H-bond). Unlike conventional nondirectional interactions (e.g., ionic bonds) and lowly directional interactions (e.g., monodentate H-bonds), salt-bridge H-bonds are highly directional and accompanied by a substantial entropy penalty (Figure 1b). Experimentally, we selected a fully biobased poly(α-thioctic acid) (polyTA)/arginine SPN as an example, in which highly specific salt-bridge H-bonds are transiently formed between the oppositely charged guanidinium groups in arginine and carboxylate groups in polyTA (Figure 1c).[34−36] Owing to the competition of salt-bridge H-bonds between polyTA-arginine and arginine−arginine, the polyTA/arginine SPN possesses a hierarchical structure comprising arginine clusters and a polyTA matrix. Such a heterogeneous structure can maximize the dominance of interfacial salt-bridge H-bonds in regulating its rheological behavior.[37] Consequently, upon impact, the SPN undergoes a dramatic transition from a soft dissipating state (G' ~ 21 kPa, 0.1 Hz) to a highly stiffened glassy state (G' ~ 45.3 MPa, 100 Hz), corresponding to an exceptional storage modulus increase of ~2100 times (Figure 1d). We further elucidate the mechanism underlying the entropy-driven stiffening response of the polyTA/arginine SPN, and we demonstrate its promising applications in various impact-protective scenarios.

RESULTS AND DISCUSSION

Synthesis and Optimization of Impact-Stiffening SPNs. PolyTA/arginine SPNs were readily synthesized through a simple one-pot reaction involving molten TA and arginine, resulting in a transparent yet yellowish material with high transmittance (≈90%, Figures 1c, S1, and S2). Upon heating, the molten TA underwent spontaneous ring-opening polymerization, leading to the formation of a flexible polyTA chain with alternating disulfide bonds in the backbone.[38,39] Simultaneously, arginine molecules became dispersed within the polyTA matrix, exposing their strongly basic guanidinium groups (pK_a ~ 12.5)[40,41] that interact with the carboxylate groups of polyTA. Importantly, the formation of salt-bridge H-bonds between these two components plays a crucial role in protecting the metastable polyTA chains from inverse ring-

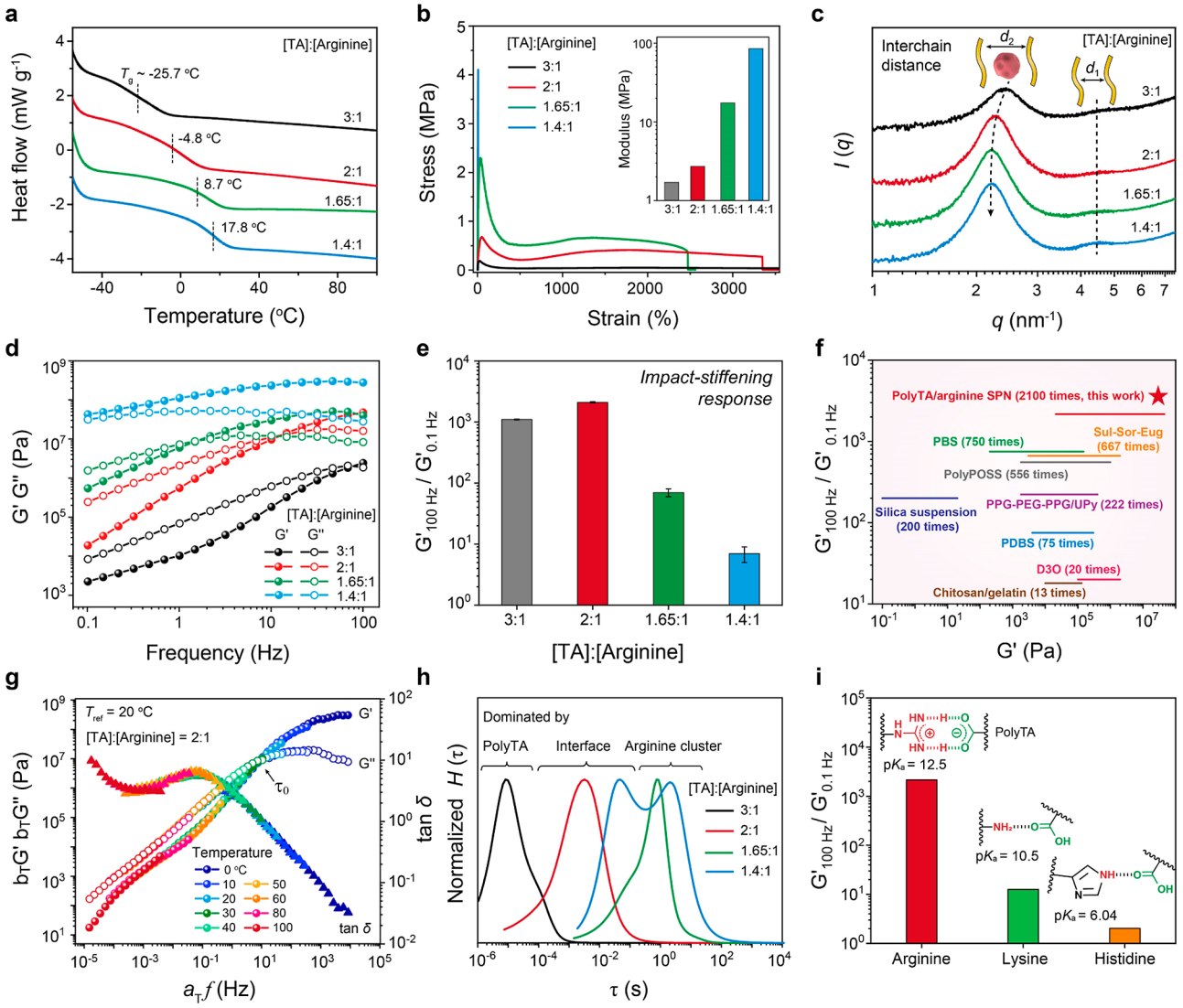

Figure 2. Optimization of the impact-stiffening response of the polyTA/arginine SPN. (a) DSC heating curves of polyTA/arginine SPNs with different molar ratios. (b) Nominal tensile stress–strain curves (strain rate: 0.34 s^{-1}; inset: calculated Young's moduli). (c) SAXS profiles with labeled interchain distances of polyTA. (d) Frequency–sweep rheological curves from 0.1 to 100 Hz. (e) Impact-stiffening response reflected by the ratio of storage modulus at 100 Hz to that at 0.1 Hz. (f) Comparison of the impact-stiffening response and storage modulus among different impact-stiffening materials (data in Table S1). (g) Time–temperature superposition rheological master curves of the SPN ([TA]/[arginine] = 2:1). (h) Converted relaxation spectra via the iterative fitting of master curves. (i) Comparison of the impact-stiffening response among polyTA/arginine, polyTA/lysine, and polyTA/histidine SPNs.

closing depolymerization.[42] It is also noted that the guanidinium-carboxylate salt-bridge H-bonds between self-associated arginine molecules (COOH, pK_a ~ 1.8) are much stronger than those between arginine and polyTA (COOH, pK_a ~ 4.7).[40,43] The competition of these two salt-bridge H-bonds leads to phase separation between arginine and polyTA, causing arginine molecules to preferentially self-aggregate into clusters.

To optimize the mechanical properties of the resulting SPNs, we meticulously adjusted the molar ratio of TA to arginine ([TA]/[arginine]). A proper amount of arginine ([TA]/[arginine] from 3:1 to 1.4:1) effectively stabilized metastable polyTA. The resulting SPNs are amorphous, as evidenced by the absence of TA crystallite peaks in X-ray diffraction profiles (XRD, Figures S3 and S4). The glass transition temperatures (T_g) of the SPNs rose from −25.7 to 17.8 °C, as determined by differential scanning calorimetry (DSC, Figure 2a). This increase in T_g is attributed to the increasing salt-bridge H-bonds between the two components, which restricted the mobility of polyTA chains. Consequently, the SPNs became less stretchable and more rigid with an increasing arginine content (Figure 2b). At a relatively low strain rate (0.34 s^{-1}), the SPNs with lower arginine contents ([TA]/[arginine] from 3:1 to 1.65:1) could be readily stretched over 20 times. Small-angle X-ray scattering (SAXS) revealed that the incorporation of self-clustering arginine increased the interchain distance of polyTA from 1.4 nm ($d_1 = 2\pi/q_1$ and q_1 = 4.5 nm^{-1}) to approximately 2.6 nm ($d_2 = 2\pi/q_2$ and q_2 = 2.4 nm^{-1}) (Figure 2c). The slightly increased d_2 values with increasing arginine contents suggest a small increase in the size of the arginine clusters. Therefore, increasing arginine content primarily led to an increase in the number of arginine clusters, consequently driving the formation of more salt-bridge H-bonds between polyTA and

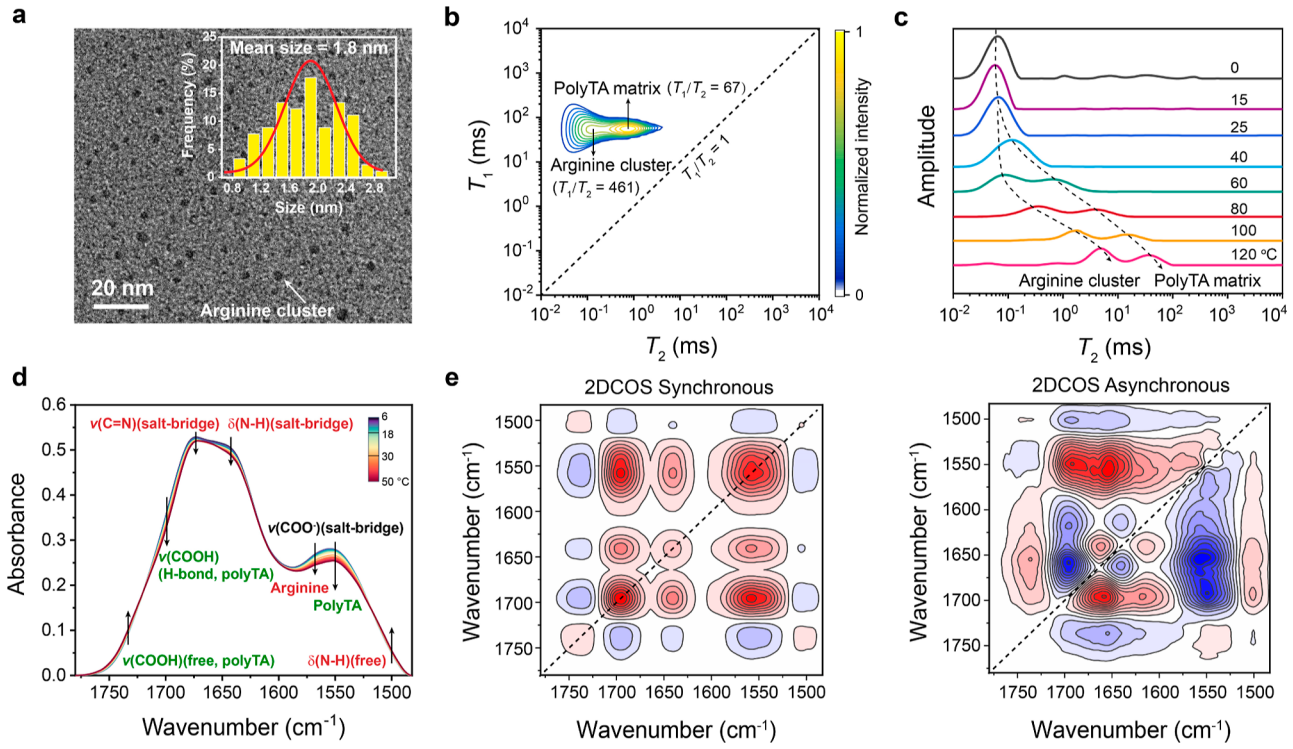

Figure 3. Mechanism characterizations for the impact-stiffening response of the polyTA/arginine SPN. (a) TEM image of the SPN shows the presence of arginine clusters with a mean size of 1.8 nm. (b) 2D low-field ^{1}H NMR spectrum at 60 °C. (c) Temperature-dependent low-field ^{1}H NMR spectra. (d) Temperature-variable FTIR spectra of the SPN upon heating from 6 to 50 °C (interval: 4 °C). (e) 2DCOS synchronous and asynchronous spectra generated from (d). In 2DCOS spectra, red colors represent positive intensities, while blue colors represent negative intensities.

arginine. This observation aligns with the subtle peak shift of ν(C═N) from arginine upon altering its content (Figure S5).

The impact-stiffening behavior of polyTA/arginine SPNs was quantitatively assessed through rheological tests conducted within the typical shear frequency range of 0.1−100 Hz (Figure 2d). All four studied SPNs exhibited an increase in storage modulus (G') as the strain rate increased. In the quasi-static state (~0.1 Hz), the SPN with a [TA]/[arginine] ratio of 1.4:1 approached the glassy regime, consistent with a measured T_g close to room temperature (17.8 °C, Figure 2a). In contrast, all the other SPNs are located in the liquid-like dissipating regime (or glass transition regime).[44] The replotted time−composition superposition master curve convincingly demonstrated a rheological transition from dissipating to glassy behavior as the arginine content increased (Figure S6). Note that this rheological transition was deliberately tailored as viscoelastic polymers in this regime often exhibit a sharp modulus response to strain rate.[45]

The impact-stiffening response was most pronounced for the SPN with a [TA]/[arginine] ratio of 2:1, in which G' increased dramatically from 21 kPa at 0.1 Hz to 45.3 MPa at 100 Hz, corresponding to a remarkable enhancement of ~2100 times (Figure 2e). This dramatic impact-stiffening response, coupled with the high modulus in the stiffened state, surpasses many previously reported impact-stiffening materials (see the comparison in Figure 2f and Table S1). Notably, the impact-stiffening response of the polyTA/arginine SPN was fully reversible without apparent hysteresis (Figures S7 and S8), highlighting its great potential for smart protective applications.

To gain a comprehensive understanding of the viscoelastic behavior of the SPNs, we further plotted rheological master curves following the time−temperature superposition principle at the reference temperature of 20 °C. The optimized SPN with a [TA]/[arginine] ratio of 2:1 exhibited a remarkable dissipating-to-glassy transition within the impact-related frequency range (Figure 2g). The Kuhn segment relaxation time (τ_0), calculated from the reciprocal of the crossover frequency, was determined to be 80 ms, sufficiently short to allow for impact-induced chain freezing and material stiffening. Additionally, the absence of a rubbery plateau indicated that there was no significant entanglement within the polyTA matrix.[46] Consistent with this observation, the number-average molecular weight of polyTA in the as-prepared SPN was merely 4.0×10^4 g mol^{-1} (Figure S9), substantially lower than that reported for elastic polyTA materials (>10^5 g mol^{-1}).[42] Furthermore, the activation energy (E_a) for chain relaxation was extracted from the horizonal shift factors as a function of temperature (Figures S10−S13). E_a increased monotonically with increasing arginine contents (Figure S13), manifesting the role of arginine clusters in restricting the chain dynamics of polyTA.

To further elucidate the relaxation mechanisms in polyTA/arginine SPNs, we employed the generalized Maxwell model to convert frequency-dependent storage and loss moduli (G' and G'') into relaxation spectra, $H(\tau)$, revealing a distinct distribution of relaxation times.[47] Increasing arginine contents led to progressively longer relaxation times, indicating slower chain dynamics (Figure 2h). Furthermore, the population within the spectra manifested three relaxation modes with increasing relaxation times: polyTA (dissipating by self-

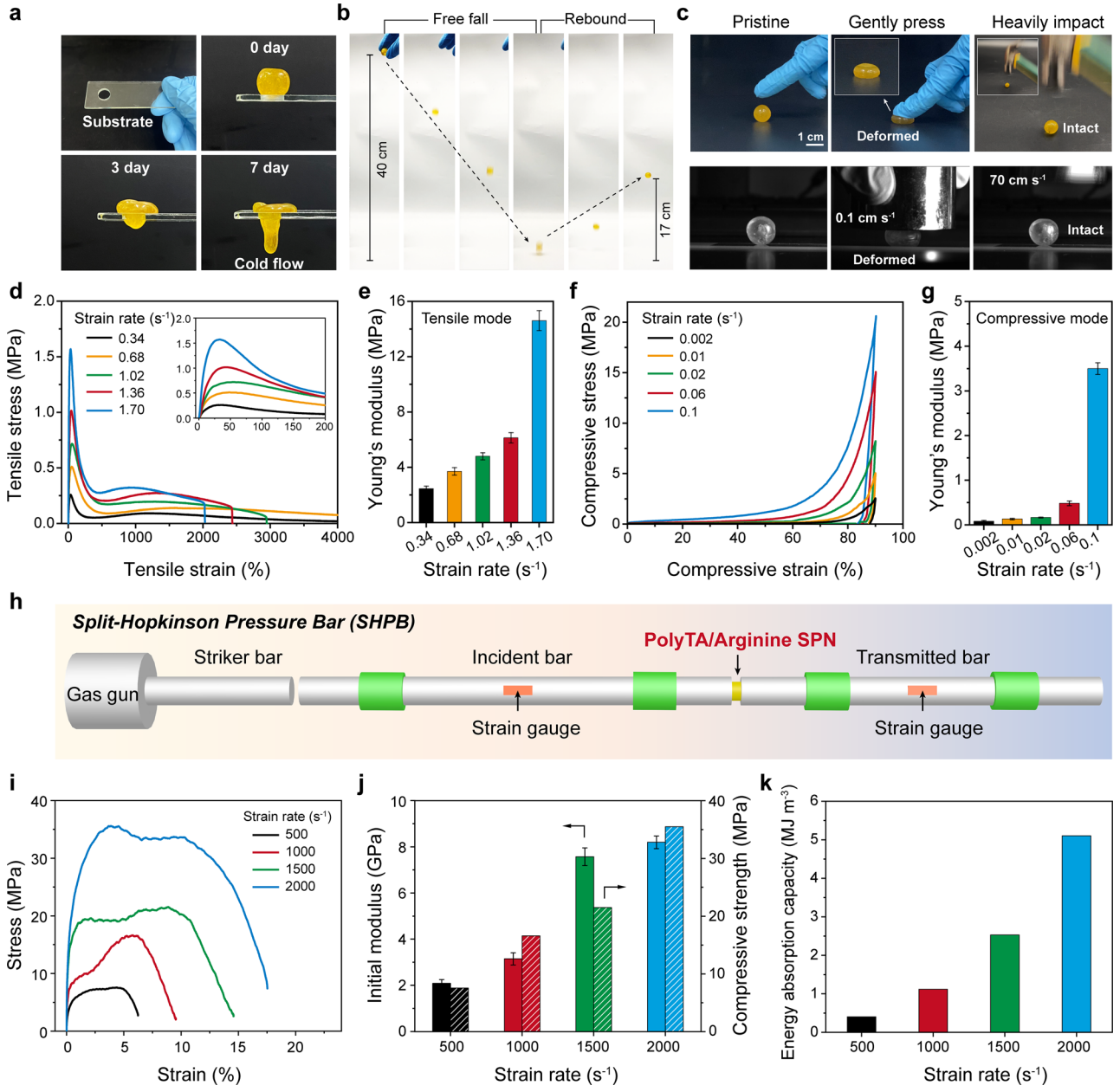

Figure 4. Strain rate-dependent mechanical properties of the polyTA/arginine SPN. (a) Pictures showing the cold flow characteristics of the SPN by placing it on a punched glass plate over 7 days. (b) Rebound elasticity of the SPN in the free-falling test. (c) Demonstration of the impact-stiffening behavior by gently pressing or heavily impacting the SPN. The bottom pictures were taken by a high-speed camera. (d,e) Tensile stress–strain curves and corresponding Young's moduli at different strain rates. (f,g) Compressive stress–strain curves and corresponding Young's moduli at different strain rates. (h) Experimental setup for the SHPB test. (i) SHPB stress–strain curves at different strain rates. (j,k) Corresponding initial moduli, compressive strengths, and energy absorption capacities.

associated dimeric H-bonds), the polyTA-arginine interface (dissipating by interfacial salt-bridge H-bonds), and arginine clusters (dissipating by self-associated salt-bridge H-bonds). Interestingly, the optimized SPN with a [TA]/[arginine] ratio of 2:1 was predominantly governed by the polyTA–arginine interface, while the other three samples contained significant contributions from either polyTA or arginine clusters. This finding unequivocally demonstrates that the impact-stiffening response of the polyTA/arginine SPN is mediated by the interfacial salt-bridge H-bonds that can be roughly described by one single Maxwell element.[48] Unless otherwise specified, all subsequent references to polyTA/arginine SPNs pertain to the sample with an optimized [TA]/[arginine] ratio of 2:1.

To further emphasize the crucial role of salt-bridge H-bonds in the impact-stiffening response of the SPN, we substituted arginine with two other basic amino acids: lysine (with an amino side group, $pK_a \sim 10.5$) and histidine (with an imidazole side group, $pK_a \sim 6.04$), both of which can only form monodentate H-bonds with polyTA.[40] Decreasing the basicity of amino acids and the entropy penalty for H-bonding largely reduced their compatibility with polyTA at the molecular level (Figure S14). Consequently, in stark contrast to polyTA/arginine SPN, both polyTA/lysine and polyTA/histidine SPNs exhibited significantly diminished impact-stiffening behavior (Figures 2i and S15).

Mechanism Discussion for the Impact-Stiffening Response. The preceding characterizations have highlighted the critical role of entropy-driven polymer−cluster interfacial interactions in the impact-stiffening response of the polyTA/arginine SPN. To substantiate this hypothesis, we employed transmission electron microscopy (TEM) and atomic force microscopy (AFM) to observe the hierarchical structure of the SPN. The captured images revealed the presence of numerous arginine clusters with a mean size of 1.8 nm (Figures 3a and S16), fully consistent with previous SAXS results. The two-phase morphology was further corroborated by 2D low-field ^{1}H NMR spectroscopy (Figures 3b and S17). The corresponding 2D T_1-T_2 plot (T_1: spin−lattice relaxation time; T_2: spin−spin relaxation time) clearly distinguished two distinct species: arginine clusters with a high T_1/T_2 ratio (=461) and polyTA matrix with a low T_1/T_2 ratio (=67). Generally, a higher T_1/T_2 ratio indicates a lower mobility (the diagonal line with T_1/T_2 = 1 represents a completely mobile liquid state).[49] It is understandable that arginine clusters are significantly less mobile than the flexible polyTA matrix and thus act as multiple physical cross-linkers that regulate the whole chain dynamics of the SPN. Such a phase-separated structure was extremely stable with almost no changes within 4 months, as evidenced by SAXS measurements (Figure S18).

To gain deeper insights into the impact-stiffening response of the polyTA/arginine SPN, we conducted temperature-dependent low-field ^{1}H NMR characterizations guided by the principle of time−temperature equivalency. As depicted in Figure 3c, the motions of arginine clusters and the polyTA matrix overlapped at temperatures below 40 °C but diverged at higher temperatures, accompanied by increased activities. Notably, this transition occurred between 25 and 40 °C, coinciding with the observation of maximum dissipation with a tan δ peak (~31.9 °C) (Figure S19). This further corroborates the notion that the impact-stiffening response of the polyTA/arginine SPN stems from the dissipating-to-glassy transition.

We also employed temperature-variable FTIR spectroscopy to evaluate the thermal sensitivities of the internal interactions in polyTA/arginine SPN. As shown in Figure 3d (see an enlarged view in Figure S20), with increasing temperature from 6 to 50 °C, the spectral intensities of all the H-bonded groups declined, while those of free groups increased, suggesting the heat-induced dissociation of both salt-bridge H-bonds and self-associated dimeric H-bonds between polyTA chains. 2D correlation spectra (2DCOS) were further generated to determine the thermal-responsive sequence of all the species. On the basis of Noda's judging rule,[50] with the consideration of both signs in the synchronous and asynchronous spectra (Figure 3e, see determination details in Table S2), the responsive order of different groups to temperature increase is as follows (→ denotes prior to or earlier than): 1614 → 1658 → 1639 → 1695 → 1736 → 1556 → 1549 → 1500 cm^{-1}, i.e., δ(O−H) (trapped H_2O in salt-bridge H-bond) → ν(C═N) (salt-bridge H-bond) → δ(N−H) (salt-bridge H-bond) → ν(COOH) (H-bond, polyTA) → ν(COOH) (free, polyTA) → ν(COO$^-$) (salt-bridge H-bond, arginine) → ν(COO$^-$) (salt-bridge H-bond, polyTA) → δ(N−H) (free). Notably, 2DCOS distinguished the presence of trace water, which is probably trapped in the salt-bridge H-bond pair.[50] The trapped water may help regulate the salt-bridge H-bond strength, which further affects the strain rate response. Indeed, we compared the stiffening response of the SPNs incubated at different humidities and found that the sample incubated at RH 50% (containing ~2 wt % water) had the highest response (Figures S21 and S22). Altogether, the earliest response of salt-bridge H-bond-related species again highlighted the dominant role of the high-entropy-penalty salt-bridge H-bond in governing the chain dynamics of the SPN.

Strain Rate-Dependent Mechanical Properties. The rheological tests have demonstrated that the polyTA/arginine SPN undergoes a dramatic dissipating-to-glassy transition as the strain rate (or shear frequency) increases. In the quasi-static state, its liquid-like dissipating nature allowed for arbitrary molding, as well as cold flow under the force of gravity within 7 days (Figure 4a). However, when a SPN ball (diameter ~1.5 cm) was freely dropped onto the floor from a height of 40 cm, it rebounded instantly to a height of 17 cm (Figure 4b), highlighting the impact-stiffening effect. Similarly, while the SPN can be easily deformed by gentle hand pressure, it remained virtually undeformed when it was subjected to heavy impact from a hammer or a weight (Figure 4c and Video S1).

To quantitatively assess the impact-stiffening properties, we investigated the strain rate-dependent mechanical behavior of the polyTA/arginine SPN in both low- and high-speed regimes. Tensile and compressive measurements at low strain rates were employed to evaluate its low-speed performance. Slowly stretching the SPN at a strain rate of 0.34 s^{-1} resulted in a low modulus (2.5 MPa) and unrecoverable plastic deformation of the sample (Figure 4d,e and Video S2). However, gradually increasing the strain rate to 1.70 s^{-1} led to reduced elongation and a significantly increased Young's modulus (14.6 MPa). Compressive tests conducted at strain rates ranging from 0.002 to 0.1 s^{-1} yielded similar results (Figure 4f,g), indicating that the impact-stiffening response is independent of the deformation mode. The dissipated energy calculated from the loading−unloading compressive curves increased from 0.32 MJ m^{-3} at 0.002 s^{-1} to 2.11 MJ m^{-3} at 0.1 s^{-1} (Figure S23). This high energy-dissipating behavior of the polyTA/arginine SPN stems from its high loss moduli (G'' = 0.25~16.7 MPa from 0.1 to 100 Hz, Figure 2d), which represents the energy dissipated as heat at a specified frequency.[51]

Furthermore, to examine the impact-stiffening behavior of the polyTA/arginine SPN in the high-speed regime, a split-Hopkinson pressure bar (SHPB) system, comprising a gas gun, a striker bar, an incident bar, and a transmitted bar,[12,20,24,52] was employed (Figure 4h). The initial high-speed stress wave (500 s^{-1}) led to the elastic deformation of the SPN, exhibiting an ultrahigh modulus of ~2 GPa (Figure 4i,j). This modulus is approximately 3 orders of magnitude higher than that observed in the low-speed regime, highlighting its dramatic stiffening behavior. Further increasing the strain rate from 500 to 2000 s^{-1} resulted in a substantial enhancement in the initial modulus and compressive strength to 8.2 GPa and 35.5 MPa, respectively. The corresponding energy absorption capacities, calculated to be 0.4 MJ m^{-3} at 500 s^{-1} and 5.1 MJ m^{-3} at 2000 s^{-1}, further corroborated the exceptional impact resistance of the SPN (Figure 4k). These findings collectively demonstrate the persistence of the impact-stiffening response of the polyTA/arginine SPN across both low- and high-speed regimes, underscoring its immense potential for real-world, impact-resistant, and energy-absorbing applications.

Self-Healing, Damping, and Impact-Resistant Applications. Leveraging the rapid chain dynamics in the dissipating state, the polyTA/arginine SPN can autonomously

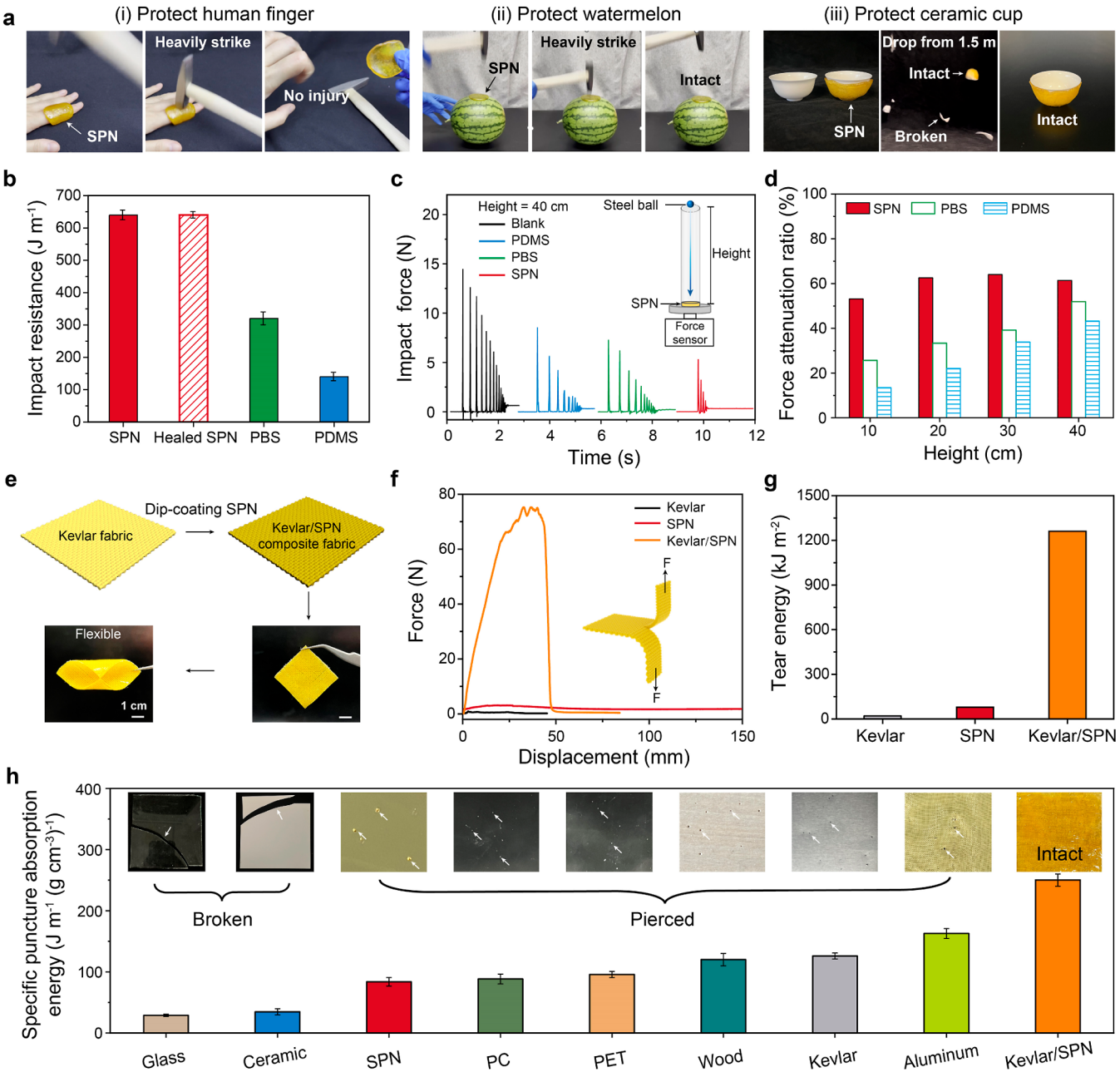

Figure 5. Impact-resistant properties of the polyTA/arginine SPN and its composite fabric. (a) The SPN can protect a human finger and a watermelon from striking (i,ii) or a ceramic cup (bone china, 0.08 mm thick) from falling (iii). The sample sizes for these three scenarios are 6 × 5 × 0.3, 5 × 5 × 0.3, and 8 × 8 × 0.1 cm^3, respectively. (b) Impact resistance of pristine and healed SPNs, PBS, and PDMS. (c) Time-resolved impact force attenuation waves transmitted through the blank sample, PDMS, PBS, and SPN when a 32 g steel ball fell freely from a height of 40 cm. (d) Corresponding impact force attenuation ratios at the heights of 10, 20, 30, and 40 cm. (e) Fabrication and photos of the Kevlar/SPN composite fabric. (f,g) Tearing force−displacement curves and corresponding tear energies of Kevlar, SPN, and the Kevlar/SPN composite fabric. (h) Specific puncture absorption energies of various impact-resistant materials.

heal damage without external intervention. For example, a scalpel-induced scar would vanish completely within 30 min at room temperature (Figure S24). The healing efficiency of the entire sample can reach nearly 100%, as demonstrated by the restored elongation and strength (Figure S25). Additionally, the polyTA/arginine SPN can be easily recycled through hot melting, and the reprocessed SPN retained all of its original mechanical properties for multiple cycles (Figure S26). Furthermore, owing to its good surface wettability and energy-dissipating properties, the polyTA/arginine SPN exhibited strong adhesion to various substrates (e.g., lap-shear strength ~11.7 MPa on aluminum), enabling its potential for adaptive protection of underlying objects (Figure S27).

All of the above intriguing properties endow the polyTA/arginine SPN with excellent buffering and impact-protective capabilities. For demonstration, we coated the SPN onto a human finger or a watermelon and struck them forcefully with a hammer without causing any injury or damage (Figure 5a-i,ii and Video S3). Similarly, we wrapped a very thin ceramic cup (thickness of ~0.8 mm) with the SPN and dropped it from a height of 1.5 m. The SPN-wrapped cup remained intact, while

the unprotected one shattered (Figure 5a-iii and Video S4). To quantitatively assess the impact resistance, we performed a drop-ball impact test (Figure 5b and Video S5). Both pristine and healed polyTA/arginine SPNs exhibited an impressive impact resistance of ~640 J m^{-1}, significantly exceeding those of PBS and PDMS (polydimethylsiloxane, a representative elastomer).

The high energy dissipation (G'' = 2.4 MPa at 1 Hz) and high loss factor (tan $\delta = G''/G'$ = 5.2 at 1 Hz) of the polyTA/arginine SPN (Figure 2g) also impart excellent impact-related vibration damping properties.[44] This can also be evaluated by the drop-ball impact test, in which a force sensor was placed under the sample to monitor the transmitted force changes. At all the studied heights (10, 20, 30, and 40 cm), the polyTA/arginine SPN could rapidly inhibit the generated shock waves, demonstrating a significantly higher damping performance than the other two control samples, PBS and PDMS (Figures 5c and S28). Moreover, the polyTA/arginine SPN reduced the impact force in the first hit with an attenuation ratio of up to 60%, also substantially higher than those of PBS and PDMS (Figure 5d).

Finally, we demonstrate that the impact-protective properties of the polyTA/arginine SPN can be further enhanced by hybridizing it with other scaffolds (e.g., Kevlar fabric) by a simple dip-coating method (Figure 5e). Notably, the relatively low viscosity of the hot-molten SPN (3.98 kPa s at 60 °C) facilitates its uniform permeation into the Kevlar fabric (Figures S29 and S30). Owing to the strong adhesion between the SPN and Kevlar fibers, the resulting composite fabric exhibited long-term stability, with no significant changes within two months (Figure S31). Despite being soft and flexible, the composite fabric exhibited exceptionally high tear resistance. The measured tear energy of the composite fabric reached 1.26 MJ m^{-2}, far exceeding those of the individual components (Figure 5f,g). This was further corroborated by the yarn pull-out test, in which the composite fabric demonstrated a pull-out force 200 times higher than that of neat Kevlar fabric (Figure S32). The combined high tear and impact resistance endows the composite fabric with outstanding puncture-resistant properties. As shown in Figure 5h, the calculated specific puncture absorption of the composite fabric was 260 J m^{-1} (g $cm^{-3})^{-1}$, surpassing not only its parent materials (Kevlar and SPN) but also numerous common protective materials, such as glass, ceramic, PC, PET, wood, and aluminum sheets. When subjected to the same puncturing impact by a dart, no visible damage was observed for the composite fabric, while the other materials were either broken or pierced with the appearance of holes. These findings together revealed the immense potential of the polyTA/arginine SPN and its composite fabric in impact-protective applications.

CONCLUSIONS

In this work, we demonstrate a key strategy to achieve a high impact-stiffening response in supramolecular materials by leveraging high-entropy-penalty physical interactions. A biobased polyTA/arginine SPN is designed as a proof-of-concept material in which a polyTA matrix is physically cross-linked by arginine clusters through highly specific salt-bridge hydrogen bonds. Owing to the dominant role of salt-bridge hydrogen bonds in regulating chain dynamics, the SPN can reversibly switch its stiffness from a soft dissipating state to a rigid glassy state upon impact, resulting in an ultrahigh stiffening response of ~2100 times. We further explored the strain rate-dependent stiffening behavior of the SPN in both low- and high-speed regimes, demonstrating its remarkable adaptability to a wide range of impact conditions. Additionally, the SPN exhibits excellent self-healing, recycling, damping, and adhesive properties. These intriguing features collectively endow the SPN and its composite fabric with superhigh impact resistance against various types of damage, including striking, shocking, and puncturing. We believe that the strategy of high-entropy-penalty design can be easily extended to other supramolecular materials, opening up new avenues for developing smart impact protectors with superior performance.

ASSOCIATED CONTENT

Supporting Information

The Supporting Information is available free of charge at

Experimental details and additional data (PDF)
Strain rate-dependent response by compressing (MP4)
Strain rate-dependent response by stretching (MP4)
Impact protection from striking (MP4)
Impact protection from falling (MP4)
Drop-ball impact test (MP4)

AUTHOR INFORMATION

Corresponding Authors

Shengtong Sun − *State Key Laboratory for Modification of Chemical Fibers and Polymer Materials, College of Chemistry and Chemical Engineering & Center for Advanced Low-dimension Materials, Donghua University, Shanghai 201620, China;* orcid.org/0000-0001-7471-686X; Email: shengtongsun@dhu.edu.cn

Peiyi Wu − *State Key Laboratory for Modification of Chemical Fibers and Polymer Materials, College of Chemistry and Chemical Engineering & Center for Advanced Low-dimension Materials, Donghua University, Shanghai 201620, China;* orcid.org/0000-0001-7235-210X; Email: wupeiyi@dhu.edu.cn

Authors

Haiyan Qiao − *State Key Laboratory for Modification of Chemical Fibers and Polymer Materials, College of Chemistry and Chemical Engineering & Center for Advanced Low-dimension Materials, Donghua University, Shanghai 201620, China;* orcid.org/0009-0007-3561-241X

Baohu Wu − *Jülich Centre for Neutron Science (JCNS) at Heinz Maier-Leibnitz Zentrum (MLZ) Forschungszentrum Jülich, Garching 85748, Germany;* orcid.org/0000-0002-1291-8965

Notes

The authors declare no competing financial interest.

ACKNOWLEDGMENTS

The authors appreciate the support from the National Natural Science Foundation of China (NSFC) (nos. 52322306, 21991123, 22275032, and 52161135102). S.S. also thanks the support from the Shanghai Talent Development Fund (no. 2021021).

REFERENCES

(1) Doolan, J. A.; Alesbrook, L. S.; Baker, K.; Brown, I. R.; Williams, G. T.; Hilton, K. L. F.; Tabata, M.; Wozniakiewicz, P. J.; Hiscock, J. R.; Goult, B. T. Next-generation protein-based materials capture and preserve projectiles from supersonic impacts. *Nat. Nanotechnol.* **2023**, *18* (9), 1060−1066.

(2) Yin, Z.; Hannard, F.; Barthelat, F. Impact-resistant nacre-like transparent materials. *Science* **2019**, *364* (6447), 1260−1263.

(3) Liang, X.; Chen, G.; Lei, I. M.; Zhang, P.; Wang, Z.; Chen, X.; Lu, M.; Zhang, J.; Wang, Z.; Sun, T.; Lan, Y.; Liu, J. Impact-resistant hydrogels by harnessing 2D hierarchical structures. *Adv. Mater.* **2023**, *35* (1), 2207587.

(4) Xu, Z.; Wu, M.; Gao, W.; Bai, H. A sustainable single-component "silk nacre". *Sci. Adv.* **2022**, *8* (19), No. eabo0946.

(5) Xiong, R.; Wu, W.; Lu, C.; Cölfen, H. Bioinspired chiral template guided mineralization for biophotonic structural materials. *Adv. Mater.* **2022**, *34* (51), 2206509.

(6) Chen, S.-M.; Gao, H.-L.; Zhu, Y.-B.; Yao, H.-B.; Mao, L.-B.; Song, Q.-Y.; Xia, J.; Pan, Z.; He, Z.; Wu, H.-A.; Yu, S.-H. Biomimetic twisted plywood structural materials. *Natl. Sci. Rev.* **2018**, *5* (5), 703−714.

(7) Jin, B.; Ren, L.; Gou, Y.; Ma, R.; Liang, Z.; Li, Z.; Dong, B.; Zhao, L.; Wang, S.; Wu, C. Fiber-bridging-induced toughening of perovskite for resistance to crack propagation. *Matter* **2023**, *6* (5), 1622−1638.

(8) Wang, J.; Sun, S.; Wu, P. A sustainable, ultratough, and ready-to-use adhesive heating patch driven by solar/electric dual energy. *SusMat* **2021**, *1* (4), 545−557.

(9) Zhao, H.; Liu, S.; Wei, Y.; Yue, Y.; Gao, M.; Li, Y.; Zeng, X.; Deng, X.; Kotov, N. A.; Guo, L.; Jiang, L. Multiscale engineered artificial tooth enamel. *Science* **2022**, *375* (6580), 551−556.

(10) Zhao, D.; Pang, B.; Zhu, Y.; Cheng, W.; Cao, K.; Ye, D.; Si, C.; Xu, G.; Chen, C.; Yu, H. A stiffness-switchable, biomimetic smart material enabled by supramolecular reconfiguration. *Adv. Mater.* **2022**, *34* (10), 2107857.

(11) Qiu, Y.; Wu, L.; Liu, S.; Yu, W. An impact resistant hydrogel enabled by bicontinuous phase structure and hierarchical energy dissipation. *J. Mater. Chem. B* **2023**, *11* (4), 905−913.

(12) Wu, Y.; Wang, Y.; Guan, X.; Zhang, H.; Guo, R.; Cui, C.; Wu, D.; Cheng, Y.; Ge, Z.; Zheng, Y.; Zhang, Y. Molecular clogging organogels with excellent solvent maintenance, adjustable modulus, and advanced mechanics for impact protection. *Adv. Mater.* **2023**, *35* (48), 2306882.

(13) Zhao, C.; Gong, X.; Wang, S.; Jiang, W.; Xuan, S. Shear stiffening gels for intelligent anti-impact applications. *Cell Rep. Phys. Sci.* **2020**, *1* (12), 100266.

(14) Liu, Z.; Picken, S. J.; Besseling, N. A. M. Polyborosiloxanes (PBSs), synthetic kinetics, and characterization. *Macromolecules* **2014**, *47* (14), 4531−4537.

(15) Brown, E.; Forman, N. A.; Orellana, C. S.; Zhang, H.; Maynor, B. W.; Betts, D. E.; DeSimone, J. M.; Jaeger, H. M. Generality of shear thickening in dense suspensions. *Nat. Mater.* **2010**, *9* (3), 220−224.

(16) Chen, D. Z.; Zheng, H.; Wang, D.; Behringer, R. P. Discontinuous rate-stiffening in a granular composite modeled after cornstarch and water. *Nat. Commun.* **2019**, *10* (1), 1283.

(17) Wang, W.; Wang, S.; Zhou, J.; Deng, H.; Sun, S.; Xue, T.; Ma, Y.; Gong, X. Bio-inspired semi-active safeguarding design with enhanced impact resistance via shape memory effect. *Adv. Funct. Mater.* **2023**, *33* (13), 2212093.

(18) Wu, Q.; Peng, Y.; Xiong, H.; Hou, Y.; Cai, M.; Wang, Y.; Zhao, L.; Wu, J. A novel shear-stiffening supramolecular material derived from diboron structure. *Sci. China Mater.* **2023**, *66* (11), 4489−4498.

(19) D'Elia, E.; Barg, S.; Ni, N.; Rocha, V. G.; Saiz, E. Self-healing graphene-based composites with sensing capabilities. *Adv. Mater.* **2015**, *27* (32), 4788−4794.

(20) Wang, C.; Lei, G.; Zhang, R.; Zhou, X.; Cui, J.; Shen, Q.; Luo, G.; Zhang, L. Shear-thickening covalent adaptive networks for bifunctional impact-protective and post-tunable tactile sensors. *ACS Appl. Mater. Interfaces* **2023**, *15* (1), 2267−2276.

(21) Wu, J.; Wang, Y.; Zhang, J.; Zhao, C.; Fan, Z.; Shu, Q.; He, X.; Xuan, S.; Gong, X. A lightweight aramid-based structural composite with ultralow thermal conductivity and high-impact force dissipation. *Matter* **2022**, *5* (7), 2265−2284.

(22) Liu, J.; Sheng, Z.; Zhang, M.; Li, J.; Zhang, Y.; Xu, X.; Yu, S.; Cao, M.; Hou, X. Non-newtonian fluid gating membranes with acoustically responsive and self-protective gas transport control. *Mater. Horiz.* **2023**, *10* (3), 899−907.

(23) Liu, K.; Cheng, L.; Zhang, N.; Pan, H.; Fan, X.; Li, G.; Zhang, Z.; Zhao, D.; Zhao, J.; Yang, X.; Wang, Y.; Bai, R.; Liu, Y.; Liu, Z.; Wang, S.; Gong, X.; Bao, Z.; Gu, G.; Yu, W.; Yan, X. Biomimetic impact protective supramolecular polymeric materials enabled by quadruple H-bonding. *J. Am. Chem. Soc.* **2021**, *143* (2), 1162−1170.

(24) Yin, J.-F.; Xiao, H.; Xu, P.; Yang, J.; Fan, Z.; Ke, Y.; Ouyang, X.; Liu, G. X.; Sun, T. L.; Tang, L.; Cheng, S. Z. D.; Yin, P. Polymer topology reinforced synergistic interactions among nanoscale molecular clusters for impact resistance with facile processability and recoverability. *Angew. Chem., Int. Ed.* **2021**, *60* (41), 22212−22218.

(25) Zhou, X.; Yang, J.; Yang, J.; Yin, P. Topological interaction among molecular cluster assemblies affords tunable viscoelasticity. *J. Phys. Chem. Lett.* **2022**, *13* (30), 7009−7015.

(26) Hou, K.-X.; Zhao, P.-C.; Duan, L.; Fan, M.; Zheng, P.; Li, C.-H. Bitumen-like polymers prepared via inverse vulcanization with shear stiffening and self-healing abilities for multifunctional applications. *Adv. Funct. Mater.* **2023**, *33* (51), 2306886.

(27) Wang, D.; Xu, J.; Chen, J.; Hu, P.; Wang, Y.; Jiang, W.; Fu, J. Transparent, mechanically strong, extremely tough, self-recoverable, healable supramolecular elastomers facilely fabricated via dynamic hard domains design for multifunctional applications. *Adv. Funct. Mater.* **2020**, *30* (3), 1907109.

(28) Huang, Z.; Chen, X.; O'Neill, S. J. K.; Wu, G.; Whitaker, D. J.; Li, J.; McCune, J. A.; Scherman, O. A. Highly compressible glass-like supramolecular polymer networks. *Nat. Mater.* **2022**, *21* (1), 103−109.

(29) Wu, S.; Chen, Q. Advances and new opportunities in the rheology of physically and chemically reversible polymers. *Macromolecules* **2022**, *55* (3), 697−714.

(30) Yu, A. C.; Lian, H.; Kong, X.; Lopez Hernandez, H.; Qin, J.; Appel, E. A. Physical networks from entropy-driven non-covalent interactions. *Nat. Commun.* **2021**, *12* (1), 746.

(31) Jin, Z.; Chen, T.; Liu, Y.; Feng, W.; Chen, L.; Wang, C. Multivalent design of low-entropy-penalty ion-dipole interactions for dynamic yet thermostable supramolecular networks. *J. Am. Chem. Soc.* **2023**, *145* (6), 3526−3534.

(32) Schneider, H.-J. Binding mechanisms in supramolecular complexes. *Angew. Chem., Int. Ed.* **2009**, *48* (22), 3924−3977.

(33) Marco-Dufort, B.; Iten, R.; Tibbitt, M. W. Linking molecular behavior to macroscopic properties in ideal dynamic covalent networks. *J. Am. Chem. Soc.* **2020**, *142* (36), 15371−15385.

(34) Mogaki, R.; Hashim, P. K.; Okuro, K.; Aida, T. Guanidinium-based "molecular glues" for modulation of biomolecular functions. *Chem. Soc. Rev.* **2017**, *46* (21), 6480−6491.

(35) Vazdar, M.; Heyda, J.; Mason, P. E.; Tesei, G.; Allolio, C.; Lund, M.; Jungwirth, P. Arginine "magic": Guanidinium like-charge ion pairing from aqueous salts to cell penetrating peptides. *Acc. Chem. Res.* **2018**, *51* (6), 1455−1464.

(36) Debnath, K.; Las Heras, K.; Rivera, A.; Lenzini, S.; Shin, J.-W. Extracellular vesicle-matrix interactions. *Nat. Rev. Mater.* **2023**, *8* (6), 390−402.

(37) Wu, J.; Wu, B.; Xiong, J.; Sun, S.; Wu, P. Entropy-mediated polymer-cluster interactions enable dramatic thermal stiffening hydrogels for mechanoadaptive smart fabrics. *Angew. Chem., Int. Ed.* **2022**, *61* (34), No. e202204960.

(38) Zhang, Q.; Shi, C.-Y.; Qu, D.-H.; Long, Y.-T.; Feringa, B. L.; Tian, H. Exploring a naturally tailored small molecule for stretchable, self-healing, and adhesive supramolecular polymers. *Sci. Adv.* **2018**, *4* (7), No. eaat8192.

(39) Zhang, Q.; Qu, D.-H.; Feringa, B. L.; Tian, H. Disulfide-mediated reversible polymerization toward intrinsically dynamic smart materials. *J. Am. Chem. Soc.* **2022**, *144* (5), 2022−2033.
(40) Haynes, W. M.; Lide, D. R.; Bruno, T. J. *Handbook of Chemistry and Physics*; CRC Press, 2014.
(41) Courvoisier, E.; Williams, P. A.; Lim, G. K.; Hughes, C. E.; Harris, K. D. M. The crystal structure of L-arginine. *Chem. Commun.* **2012**, *48* (22), 2761−2763.
(42) Wang, Y.; Sun, S.; Wu, P. Adaptive ionogel paint from room-temperature autonomous polymerization of α-thioctic acid for stretchable and healable electronics. *Adv. Funct. Mater.* **2021**, *31* (24), 2101494.
(43) Reed, L. J.; DeBusk, B. G.; Gunsalus, I. C.; Schnakenberg, G. H. F. Chemical nature of α-lipoic acid. *J. Am. Chem. Soc.* **1951**, *73* (12), 5920.
(44) Xiang, H.; Li, X.; Wu, B.; Sun, S.; Wu, P. Highly damping and self-healable ionic elastomer from dynamic phase separation of sticky fluorinated polymers. *Adv. Mater.* **2023**, *35* (10), 2209581.
(45) Shi, Y.; Wu, B.; Sun, S.; Wu, P. Peeling-stiffening self-adhesive ionogel with superhigh interfacial toughness. *Adv. Mater.* **2023**, *35*, 2310576.
(46) Daniel, W. F. M.; Burdyńska, J.; Vatankhah-Varnoosfaderani, M.; Matyjaszewski, K.; Paturej, J.; Rubinstein, M.; Dobrynin, A. V.; Sheiko, S. S. Solvent-free, supersoft and superelastic bottlebrush melts and networks. *Nat. Mater.* **2016**, *15* (2), 183−189.
(47) Ferry, J. D. *Viscoelastic Properties of Polymers*; John Wiley & Sons, 1980.
(48) Grindy, S. C.; Learsch, R.; Mozhdehi, D.; Cheng, J.; Barrett, D. G.; Guan, Z.; Messersmith, P. B.; Holten-Andersen, N. Control of hierarchical polymer mechanics with bioinspired metal-coordination dynamics. *Nat. Mater.* **2015**, *14* (12), 1210−1216.
(49) Song, Y.-Q.; Kausik, R. NMR application in unconventional shale reservoirs - a new porous media research frontier. *Prog. Nucl. Magn. Reson. Spectrosc.* **2019**, *112*−*113* (1), 17−33.
(50) Zhang, W.; Wu, B.; Sun, S.; Wu, P. Skin-like mechanoresponsive self-healing ionic elastomer from supramolecular zwitterionic network. *Nat. Commun.* **2021**, *12* (1), 4082.
(51) Sperling, L. H. Sound and Vibration Damping with Polymers: Basic Viscoelastic Definitions and Concepts. In *Sound and Vibration Damping with Polymers*; American Chemical Society, 1990, pp 5−22.
(52) Felten, M.; Fries, M.; Fíla, T.; Zlámal, P.; Falta, J.; Jiroušek, O.; Jung, A. High strain-rate compression experiments on Ni/polyurethane hybrid metal foams using the split-hopkinson pressure bar technique. *Adv. Eng. Mater.* **2022**, *24* (3), 2100872.

https://doi.org/10.1021/jacs.3c13392
J. Am. Chem. Soc. XXXX, XXX, XXX−XXX